New Approach to Predict Shear Capacity of Reinforced Concrete Beams Strengthened with NSM Technique

Hadi Baghi, Joaquim A.O. Barros

Abstract

Understanding the shear behavior of a concrete beam is still a challenging task due to several complex mechanisms it involves. The modified compression field theory (MCFT) demonstrated to be able of predicting with good accuracy the shear capacity of reinforced concrete (RC) members. Due to its iterative nature, the MCFT is not a straightforward design methodology, and a simplified MCFT (SMCFT) approach of this method was proposed to overcome this aspect. This model takes into account the tensile stress installed in the cracked concrete, and inclination of the diagonal compressive strut, and requires a smaller number of model parameters than MCFT.

This paper presents a new approach to predict the shear capacity of RC beams shear strengthened with fiber reinforced polymer (FRP) laminates/rods applied according to the near surface mounted (NSM) technique. The new approach is based on the SMCFT and considers the relevant features of the interaction between NSM FRP systems and surrounding concrete like debonding of FRP laminate/rod and fracture of surrounding concrete of FRP. The experimental results of 100 beams strengthened with different configurations and shear strengthening ratio of FRP reinforcements are used to appraise the predictive performance of the developed approach. By evaluating the ratio between the experimental results to the analytical predictions ($V_{\exp.} / \mathrm{V}_{ana.}$), an average value 1.09 is obtained for the developed approach with a coefficient of variation of 11%.

Keywords: Simplified Modified Compression Field Theory; Reinforced concrete beams; Shear failure; Shear strengthening; Near Surface Mounted technique; Carbon fiber reinforced polymers.

Biography:

Hadi Baghi got a PhD degree in June 2015 in the Department of Civil Engineering of Minho University. His research interests involve the use of strain hardening cement composites and fiber reinforced polymer systems, advanced numerical modeling and design guidelines for the structural rehabilitation.

Joaquim A. O. Barros is Full Professor of the Department of Civil Engineering of Minho University and coordinator of the Structural Composites Group. He is a member of several ACI, fib and RILEM technical committees. His research interests include structural strengthening, composite materials, fiber reinforced concrete and the development of constitutive models for the simulation of the behavior of cement based and polymer based materials, and their implementation in software based on the finite element method (FEM). He is the co-founder of FEMIX FEM-based computer program for advanced structural analysis, and founder of the CiviTest Company (www.civitest.pt).

Introduction

The prediction of the shear capacity of reinforced concrete (RC) beams is still a challenging task because shear mobilizes several complex resisting mechanisms namely: (a) shear resistance developed by the uncracked concrete in the compression zone (V_c); (b) interface shear transfer by aggregate interlocking in the cracked concrete (V_a); and (c) dowel action of the longitudinal reinforcement (V_d) (**Fig. 1**) [1]. There are two prominent approaches that have been used to predict the shear strength of RC beams: Truss Model (TM) and Modified Compression Field Theory (MCFT).

Truss model was explained by Ritter (1899) and Mörsch (1908) [2], which is based on the following two assumptions: 1) the diagonal compression struts, before and after cracking of the cross section, are inclined at an angle of 45 degrees to the longitudinal axis of the RC member; 2) the concrete tensile strength is negligible [2]. Hence, the truss model predicts conservative values for the ultimate shear strength of the RC elements since smaller inclinations can occur (crossing larger number of stirrups), and concrete post-cracking tensile strength can be significant.

The Modified Compression Field Theory (MCFT) was developed by Vecchio and Collins [3] by taking into account the resisting contribution of cracked RC member in tension. By applying this theory for the prediction of the shear strength of 102 panels tested experimentally, an average predictive level of 1.01 (ratio between experimental and model results), with a coefficient of variation (COV) of 12.2%, was obtained [4]. Nevertheless, solving the equations of the MCFT requires an iterative procedure and the knowledge of a relatively high number of parameters, which introduces extra difficulties in the designer perspective.

Bentz *et al.* [4] suggested a simplified approach of the MCFT method. In this model, the shear strength of a section is a function of two parameters: the tensile stress factor in the cracked concrete (β), and the inclination of the diagonal compressive stress in the web of the section (θ). In spite of the simple format of the equations for β and θ, the method provides excellent predictions of shear strength of RC beams. In the simplified MCFT (SMCFT), the average ratio of experimental to predicted shear strength for 102 RC elements was 1.11 with a COV of 13.0% [4].

Shear failure of RC elements due to design deficiency is brittle, and several strengthening techniques are being proposed to avoid this type of rupture, such as the near surface mounted (NSM). In this technique, carbon fiber reinforced polymer (CFRP) laminates/rods are inserted into grooves open on the concrete cover, and bonded to the surrounding substrata by using an appropriate adhesive. Research has shown that a significant increase in the shear resistance of RC beams is reachable by using the NSM CFRP technique [5, 6].

Nanni *et al.* [7] and Bianco *et al.* [8] are two amongst the most consistent models proposed to predict the shear strength contribution of the NSM CFRP laminate/rod in RC beams. In the Nanni *et al.* model the inclination of the critical diagonal crack (CDC) with respect to the axis of the beam (θ) was assumed constant and equal to 45 degrees, which limits the predictive performance of this model. One of the input parameters in Bianco *et al.* approach is the inclination of the CDC. However, due to lack of an appropriate approach to predict the θ, this model gives conservative estimates of the shear strength contribution of the NSM laminate/rod. In fact, when applied to an experimental program formed by 72 RC beams, the average ratio of the prediction versus the experimental value was 0.69 with a COV of 42% [8].

In the present paper a model based on the Simplified MCFT and Bianco *et al.* formulation is proposed (herein abbreviated by BSMCFT) to predict the shear capacity of RC beams shear strengthened according to the NSM technique. In the first part of this paper, the SMCFT and the Bianco *et al.* are briefly introduced. To appraise the predictive performance of the developed approach, it is applied on the prediction of the shear capacity of beams shear strengthened with the NSM technique and tested experimentally.

Research Significance

An analytical model is developed to predict shear strength of reinforced concrete beams strengthened with the Near Surface Mounted (NSM) FRP laminate/rod. This model integrates the relevant features of the Simplified Modified Compression Field Theory (SMCFT) and the key mechanisms provided by FRP reinforcements applied according to the NSM technique for the shear strengthening of RC beams, namely: 1) debonding of FRP reinforcements; 2) fracture of concrete surrounding FRPs; 3) tensile rupture of FRP reinforcements; 4) inclination of the shear crack. The results of 100 beams with and without existing shear reinforcement and with and without CFRP laminates are summarized, and the predictive performance of the new design approach is appraised, having been obtained an average of 1.09 with a COV of 11%.

Simplified Modified Compression Field Theory

In 1929 Wanger developed the Tension Field Theory (TFT) in analogy to the post-buckling shear resistance of thin-webbed metal girder [9]. In this theory it was assumed that after the thin-webbed girder buckled, it had no resistance to compression, and the shear was carried out by diagonal tension. It was also assumed that the inclination of the diagonal tensile stresses coincided with the inclination of the principal tensile strains [9]. Vecchio and Collins [3] applied the TFT to the RC members by assuming that, after cracking, the concrete carried no tension, and the shear was carried out by a field of diagonal compressive stresses. Since the Compression Field Theory (CFT) neglects the resisting contribution of cracked concrete in tension, conservative estimates of shear strength were predicted. The Modified Compression Field Theory (MCFT) is an enhancement of the CFT, since it takes into account the resisting contribution of the cracked concrete in tension [3]. Vecchio and Collins [3] studied the relationship between diagonal compressive stress and diagonal compressive strain, and authors found that principal compressive stress was not only function of the principal compressive strain but also principal stresses and strains have almost the same orientation. They also verified that after formation of diagonal cracking, tensile stresses still exist in the concrete between cracks. Combined with shear stresses on the crack faces, these tensile stresses increased the ability of the cracked RC concrete to resist shear. However, due to huge amount of variables and assumptions, solving the equations of the MCFT is cumbersome if done by hand [10].

Bentz *et al.* [4] suggested a simplified approach of the MCFT method, where the shear strength of a section is a function of two parameters: the tensile stress factor in the cracked concrete (β), and the inclination of the diagonal compressive stress in the web of the section (θ). For elements without transverse reinforcement the β value, depends on longitudinal strain (ε_x) and crack spacing parameter (s_{xe}). The θ and β are the results of the multiplication of ε_x and s_{xe}, the first one (ε_x) simulating the "strain effect" and the second (s_{xe}) the "size effect".

These two effects are not really independent, but for the simplified calculation of the SMCFT this interdependence is ignored. The equations 1 and 2 were suggested to calculate θ and β, respectively.

$$\theta = \left(29 + 7000\varepsilon_x\right).\left(0.88 + \frac{s_{xe}}{2500}\right) \leq 75° \tag{1}$$

$$\beta = \frac{0.4}{1 + 1500\varepsilon_x}.\frac{1300}{1000 + s_{xe}} \tag{2}$$

These two equations are to be used with concrete strength units in MPa and s_{xe} in mm. If in.-lb units are used the 2500 in equation 1 becomes 100, 1300 in equation 2 becomes 51, and the 1000 becomes 39. For concrete strength in psi, the 0.4 in equation 2 becomes 4.8.

s_{xe} can be determined by equation 3:

$$s_{xe} = \frac{35 s_x}{a_g + 16} \geq 0.85 s_x \tag{3}$$

where s_x and a_g are the vertical distance between longitudinal reinforcement and maximum dimension of aggregates, respectively, both in mm. If in.-lb units are being used, the 35 and 16 in equation 3 should be replaced by 1.38 and 0.63, respectively [4].

If the longitudinal reinforcement is not yielded, equation 4 can be used to calculate the ε_x:

$$\varepsilon_x = \frac{f_{sx}}{E_s} = \frac{v.\cot\theta - v_c / \cot\theta}{E_s \rho_{sx}} \tag{4}$$

where E_s, ρ_{sx}, v_c and v are the modulus of elasticity of longitudinal reinforcement, longitudinal steel reinforcement percentage, shear stress in concrete, and shear stress of a RC member, respectively. In Simplified MCFT, the shear strength of a RC beam can be determined as follows (equation 5):

$$v = v_c + v_s = \beta\sqrt{f_c^{'}} + \rho_y f_{y\,yield}\cot\theta \tag{5}$$

where $v_s = \rho_y f_{y\,yield}\cot\theta$ is the shear strength provided by steel stirrups. In equation 5 $f_c^{'}$ is the concrete compressive strength, while ρ_y and $f_{y\,yield}$ are the ratio, and the yield stress of the transverse steel reinforcement, respectively. More information about MCFT and SMCFT can be found in Baghi [10].

Model for the evaluation of the shear strength contribution of NSM laminate/rod

Bianco *et al.* [11] proposed a 3D mechanical model to predict the shear strength contribution of NSM CFRP laminates/rods. The mode of failure of an NSM FRP laminate/rod subjected to an imposed end slip can be categorized into four groups: debonding, tensile rupture of laminate, concrete semi-cone tensile fracture, and a mixed shallow semi-cone plus debonding failure mode (**Fig. 2d**). Recently the same authors proposed a simplified version of this model [8] by introducing the following simplifications:

1. The local bond stress-slip relationship $\tau(\delta)$ can be modeled by a bi-linear diagram instead of a multi linear diagram.
2. Concrete fracture surface is assumed a semi-pyramid instead of a semi-cone.

3. Attention can be focused on the average-available-bond-length NSM FRP laminates/rods glued on the relevant prism of surrounding concrete instead of local bond between NSM FRP laminates/rods embedded in concrete cover.
4. Determining the constitutive law of the average-available-bond-length of the NSM FRP laminates/rods instead of constitutive laws of local bond between NSM FRP laminates/rods and surrounding concrete.

During the loading process of a RC beam, when the concrete average tensile strength is attained at the bottom part of the web, some shear cracks originate, and successively progress towards the flange of the beam. These cracks can generate a single crack, Critical Diagonal Crack (CDC), with inclination of θ with respect to the beam longitudinal axis (**Fig. 2a**). At load step t_1, the two web parts become separated by the CDC and they start moving apart by rotating around the crack tip (point E in **Fig. 2a**). From that step, by increasing the applied load, the CDC opening angle $\gamma\left(t_n\right)$ progressively widens. The laminates that bridge the CDC offer resistance to its widening. The load imposed to the laminate, in consequence of the loaded end slip (δ_{Li}) evolution, is transferred by bond to the concrete surrounding the laminate along its effective bond length, L_{fi} which is the shorter length between the two parts into which the crack divides its actual length.

There are two other assumptions that simplify the original formulation proposed by Bianco *et al.*:

The concrete fracture can be accounted to determine the equivalent value of the average resisting bond length $\overline{L}_{Rfi}^{eq}$. The equivalent value of the average resisting bond length is the portion of the available average resisting bond length, $\overline{L}_{Rfi}^{eq} = \eta \overline{L}_{Rfi}$.

The post peak behavior of the bond based constitutive law $V_{fi}^{bd}(\overline{L}_{Rfi}^{eq};\delta_{Li})$ of the equivalent value of the average resisting bond length can be ignored.

The following paragraphs introduce the formulation of this approach:

Step 1: Input parameters data includes: beam cross section (h_w, b_w); inclination of CDC and NSM FRP laminates (θ, θ_f); horizontal spacing of NSM FRP laminates s_f; angle α between axis and principal surfaces that generate the semi-pyramidal fracture surface; Young's modulus and tensile strength of FRP (E_f, f_{fu}); concrete average compressive strength $(f_c^{'})$; thickness and width of the NSM FRP laminates (a_f, b_f); the value of the bond strength and ultimate slip (τ_0, δ_1) (these values are assumed 20.1 MPa [2.9 ksi] and 7.12 mm [0.28 in], respectively [11]).

Step 2: Determining the average available resisting bond length and the minimum integer number of FRP laminates/rods that cross the CDC (**Fig. 2a**):

$$\overline{L}_{Rfi} = \frac{h_w . \sin\theta . (\cot\theta + \cot\theta_f)}{4 . \sin(\theta + \theta_f)} \quad (6)$$

$$N_{f,\text{int}}^{l} = round\left[h_w . \frac{\cot\theta + \cot\theta_f}{s_f} \right] \quad (7)$$

Step 3: Evaluation of geometric constants (equation 8), mechanical constants (equation 9), and bond modeling constants (equation 10) (**Fig. 2c**):

$$L_p = 2b_f + a_f;\ A_c = s_f \frac{b_w}{2};\ L_d = \frac{h_w}{\sin\theta} \quad (8)$$

$$V_f^{tr} = a_f . b_f . f_{fu} \quad (9a)$$

$$f_{ctm} = 0.3(f_c^{'} - 8)^{2/3} \quad (9b)$$

$$E_c = 2.2 \times 10^4 (\frac{f_c'}{10})^{1/3} \quad (9c)$$

If in.-lb units are used, the 8 and 0.3 in equation 9b become 1.16 and 0.157, respectively, and 2.2×10^4 and 10 in equation 9c become 3191 and 1.45, respectively.

$$J_1 = \frac{L_p}{A_f}\left[\frac{1}{E_f} + \frac{A_f}{A_c E_c}\right] \; ; \; C_3 = \frac{V_f^{tr}.J_1}{L_p.\lambda} \; ; \; \frac{1}{\lambda^2} = \frac{\delta_1}{\tau_b J_1} \; ; \; L_{Rfe} = \frac{\pi}{2\lambda} \; ; \; V_{f1}^{bd} = \frac{L_p \lambda \delta_1}{J_1} \tag{10}$$

Step 4: Reduction factor of the initial average available resisting bond length (η), and equivalent value of the average resisting bond length ($\overline{L}_{Rfi}^{eq}$) (**Fig. 3a**):

The average resistance bond length is determined from:

$$\overline{L}_{Rfi}^{eq} = \eta.\overline{L}_{Rfi} \tag{11}$$

where:

$$\eta = \begin{cases} \dfrac{f_{ctm}}{f_{ctm}^*} & if \;\; f_{ctm} < f_{ctm}^* \\ 1 & if \;\; f_{ctm} \geq f_{ctm}^* \end{cases} \tag{12}$$

In equation 12, f_{ctm}^* representing the value of concrete average tensile strength for values larger than which concrete fracture does not occur, whose complete physical meaning is described elsewhere [11], f_{ctm}^* is determined as follow:

$$f_{ctm}^* = \frac{L_p \lambda \delta_1 \sin(\lambda.L_{Rfi})}{J_1.\min(L_{Rfi}.\tan\alpha, b_w/2).\min\left(s_f.\sin\theta_f, 2L_{Rfi}.\tan\alpha\right)} \tag{13}$$

where:

$$L_{Rfi} = \begin{cases} \overline{L}_{Rfi} & if \;\; \overline{L}_{Rfi} \leq L_{Rfe} \\ L_{Rfe} & if \;\; \overline{L}_{Rfi} > L_{Rfe} \end{cases} \tag{14}$$

Step 5: Determine the value of imposed slip in correspondence of which the comprehensive peak force transmissible by $\overline{L}_{Rfi}^{eq}$ is attained ($V_{fi}\left(\overline{L}_{Rfi}^{eq};\delta_{Li}\right)$) (**Fig. 3c**):

$$\delta_{Lu} = \begin{cases} \delta_{L1}\left(\overline{L}_{Rfi}^{eq}\right) & if \;\; V_{f1}^{db} < V_f^{tr} \\ \min\left[\delta_{L1}\left(\overline{L}_{Rfi}^{eq}\right); \delta_{Li}\left(V_f^{tr}\right)\right] & if \;\; V_{f1}^{db} \geq V_f^{tr} \end{cases} \tag{15}$$

where $\delta_{L1}\left(\overline{L}_{Rfi}^{eq}\right)$ is the value of imposed end slip in correspondence of which the bond-based constitutive law $V_{fi}^{bd}\left(\overline{L}_{Rfi}^{eq};\delta_{Li}\right)$ attains the peak value (**Fig. 3b**):

$$\delta_{L1}\left(\overline{L}_{Rfi}^{eq}\right)=\begin{cases}\delta_1[1-\cos\left(\lambda\overline{L}_{Rfi}^{eq}\right)] & if \quad \overline{L}_{Rfi}^{eq}\le L_{Rfe}\\ \delta_1 & if \quad \overline{L}_{Rfi}^{eq}> L_{Rfe}\end{cases} \tag{16}$$

and $\delta_{Li}\left(V_f^{tr}\right)$ is the imposed end slip in correspondence of which the strip tensile strength is attained:

$$\delta_{Li}\left(V_f^{tr}\right)=\delta_1\left\{1-\cos\left[-\arcsin\frac{C_3}{\delta_1}\right]\right\} \tag{17}$$

Step 6: Maximum effective capacity $V_{fi,eff}^{\max}$ of the FRP laminate/rod with equivalent average resisting bond length $\overline{L}_{Rfi}^{eq}$ (**Fig. 3c**):

The $V_{fi,eff}^{\max}$ is evaluated by neglecting the post peak behavior of the equivalent average resisting bond length (**Fig. 3b** and **3c**), whose complete physical meaning is described elsewhere [8].

$$V_{fi,eff}^{\max}=\frac{\delta_1 A_2}{2L_d A_3\gamma_{\max}}\left[\frac{\pi}{2}-\arcsin\psi-\psi\sqrt{1-\psi^2}\right] \tag{18}$$

where:

$$A_2=\frac{L_p\lambda}{J_1}\ ;\ A_3=\frac{\sin\left(\theta_f+\theta\right)}{2\delta_1}\ ;\ \gamma_{\max}=\frac{2\delta_{Lu}}{L_d\sin\left(\theta_f+\theta\right)}\ ;\ \psi=1-A_3.\gamma_{\max}.L_d \tag{19}$$

Step 7: Shear strength contribution provided by a system of NSM CFRP laminate/rod:

$$V_{fd}=2.N_{f,\text{int}}^{l}.V_{fi,eff}^{\max}.\sin\theta_f \tag{20}$$

Nanni et al. Design Formulation

Based on ACI design code [12], shear strength of a RC beam strengthened with FRP (herein abbreviated by NACI) can be determined by:

$$V = V_c + V_s + V_f \tag{21}$$

where V_c, V_s, and V_f are the shear strength provided by concrete, steel stirrups and FRP, respectively. The contribution of concrete and steel stirrups is obtained by the following respective equations:

$$V_c = 0.17\sqrt{f_c'}\,b_w d \tag{22}$$

$$V_s = \frac{A_{sy} f_{y\,yield}}{s} d \tag{23}$$

while the contribution of FRP is determined according to the Nanni *et al.* [7] model, whose detailed description is provided elsewhere [7, 13]. In this model the inclination of the CDC with respect to the axis of the beam is assumed 45°, and conservative values of the shear strength contribution of FRP can be predicted in case of occurring smaller inclinations of the crack due to the larger number of laminate/rod crossing the crack than expected when the aforementioned inclination is assumed.

New Approach to Determine the Shear Capacity of the RC Beams Strengthened with NSM Technique

Adapting the simplified MCFT to the NSM technique is performed by adding formulation of NSM technique, suggested by Bianco *et al.* [8], to simplified MCFT. As mentioned in the previous section, one of the input parameters in Bianco *et al.* approach is inclination of the CDC with respect to the longitudinal axis of the beam. To evaluate this parameter, the equation 1 provided by SMCFT can be used in Bianco *et al.* formulation.

The new formulation for shear strength, based on SMCFT, combined with Bianco *et al.* approach can be expressed as:

$$v = v_c + v_s + v_{fd} = \beta\sqrt{f_c^{'}} + \rho_y f_{yield}\cot\theta + 2.N_{f,\mathrm{int}}^{l}.V_{fi,eff}^{\max}.\frac{\sin\theta_f}{b_w d} \tag{24}$$

where θ and β are obtained from equations 1 and 2, respectively, while the longitudinal strain is calculated from equation 4.

The solution procedure to calculate the shear strength of the concrete beams, according to the BSMCFT, is obtained applying the following procedure (**Fig. 4)**:

Step 1: Input parameters;

Step 2: Assume a value for ε_x;

Step 3: Calculate the crack spacing using equation 3;

Step 4: Calculate θ and β using equation 1 and equation 2, respectively;

Step 5: Calculate the shear strength based on equation 24;

Step 6: Calculate the longitudinal strain, ε_x, according to equation 4 and compare to ε_x of step 1.

Return to Step 2 with ε_x that has been calculated in Step 5 until $\left|\varepsilon_x^{q+1} - \varepsilon_x^{q}\right| / \varepsilon_{y\ yield} \le 10^{-6}$;

Performance of the proposed formulation for predicting the shear capacity of RC Beams shear strengthened with NSM systems

Table 1 summarizes experimental results available in the literature in terms of RC beams shear strengthened with NSM reinforcement [5, 6, 10, 13-20]. These experimental programs include beams of different size, different longitudinal and transverse steel reinforcement ratios, and different NSM CFRP types and strengthening ratios.

The beams tested by Dias and Barros [5, 13-16] were of type T cross section with the same shear span to effective depth ratio (2.5), CFRP laminates, and epoxy adhesive. These beams differed on the amount of existing still stirrups ($\rho_{sy} = 0.1\%$ and 0.17%), percentage of longitudinal reinforcement ($\rho_{sx} = 2.8\%$ and 3.2%), and concrete compressive strength ($f_c^{'} = 18.6$, 39.7, and 31.1 MPa [2.7, 5.8, and 4.5 ksi]). These series were strengthened with different configurations of NSM strips in terms of both inclination θ_f and spacing s_f . However, the series V and VI of these authors [15] were formed by beams of a higher shear aspect ratio (3.3) and concrete average compressive strength ($f_c^{'} = 59.4$ MPa [8.6 ksi]).

Those beams were characterized by the following common geometric and mechanical parameters: $b_w = 180$ mm (7.1 in); $h_w = 300$ mm (11.8 in); $f_{fu} = 2952$ MPa (428 ksi) (for the series I, II, III, IV) and f_{fu}=2848 MPa (413 ksi) (for the series V and VI); $E_f = 166.6$ GP (24.2 Msi) (for the series IV), $E_f = 174.3$ GPa (25.3 Msi) (for the series III, V, and VI), and $E_f = 170.9$ GPa (24.8 Msi) (for series I and II); $a_f = 1.4$ mm (0.05 in); $b_f = 9.5$ mm (0.37 in) (for the series I, II, III, V and IV) and $a_f = 1.4$ mm (0.05 in); $b_f = 10$ mm (0.39 in) (for series IV).

The beams tested by Chaallal *et al.* [17] were of T cross section type, and were strengthened in shear by CFRP rods, and tested under three point bending. These beams were characterized by cross-section dimensions of $b_w = 152$ mm (6.0 in) and $h_w = 304$ mm (12.0 in). Concrete had average compressive strength of 25 MPa (3.6 ksi) and 35 MPa (5.1 ksi) in the series I and II, respectively. CFRP rods of 9.5 mm (0.37 in) diameter, with tensile strength of $f_{fu} = 1270$ MPa (184 ksi) and modulus of elasticity of $E_f = 148$ GPa (21.5 Msi), were used.

The beams tested by De Lorenzis and Nanni [6] were T cross section type and strengthened in shear with CFRP rods, and tested under four point bending. These beams were characterized by cross-section dimensions of $b_w = 150$ mm (5.9 in) and $h_w = 305$ mm (12 in). The concrete had an average compressive strength of 31 MPa (4.5 ksi). CFRP rods of nominal diameter around 9.5 mm (0.37 in), with tensile strength $f_{fu} =$ 1875 MPa (271.9 ksi) and modulus of elasticity $E_f = 104.8$ GPa (15.2 Msi), were adopted. Two different percentages of steel stirrups were used ($\rho_{sy} = 0.0\%$ and 0.26%).

The beams tested by Rizzo and De Lorenzis [18] were of rectangular cross-section type, strengthened in shear by either rods (NR) or laminates (NL), and tested under four point bending. These beams were characterized by cross-section dimensions of $b_w = 200$ mm (7.9 in) and $h_w = 210$ mm (8.3 in). The concrete had an average compressive strength of 29.3 MPa (4.2 ksi). Round CFRP rods of 8 mm (0.31 in) diameter, with tensile strength $f_{fu} = 2210$ MPa (87 ksi) and modulus of elasticity $E_f = 145.7$ GPa (21.1 Msi), were used. The laminates had cross-section dimensions $a_f = 2.0$ mm (0.07 in) and $b_f = 16.0$ mm (0.63 in), and mechanical properties of $f_{fu} = 2070$ MPa (300 ksi) and $E_f = 121.5$ GPa (17.6 Msi).

The beams tested by Islam [19] were of rectangular cross-section type, strengthened in shear with CFRP round rods and tested under four point bending. These beams were characterized by cross-section dimensions of $b_w = 254$ mm (10 in) and $h_w = 305$ mm (12 in). The concrete had an average compressive strength of 49.75 MPa (4.3 ksi). Round CFRP rods of 9 mm (0.35 in) diameter, with tensile strength $f_{fu} = 2070$ MPa (300 ksi) and modulus of elasticity $E_f = 124$ GPa (17.9 Msi), were used.

The beams tested by Baghi [10] were T cross-section type and tested under three point bending. T cross section beams had a cross section dimensions of $b_w = 180$ mm (7.1 in) and $h_w = 400$ mm (11.8 in). The length of monitored shear span, a, was 2.5 times the effective beam's depth. The concrete had an average compressive strength of 32.7 MPa (4.74 ksi). CFRP laminates of $a_f = 1.4$

(0.05 in) mm; $b_f = 10$ mm (0.39 in), with tensile strength $f_{fu} = 2620$ MPa (380 ksi) and modulus of elasticity $E_f = 150$ GPa (21.8 Msi), were used.

The RC beams tested by Cisneros *et al.* [20] were of rectangular cross-section strengthened in shear by either bars (their label starts by B) or laminates (their label starts by S) and tested under three point bending. The cross-section dimensions of the beams were b_w=200 mm and h_w=350 mm. Concrete average compressive strength ranged from $f_c^{'}$=22.84 MPa (3.3 ksi) to $f_c^{'}$=29.11 MPa (4.2 ksi). The NSM FRP bars were characterized by 8 mm diameter (0.31 in), while the laminates had cross section dimensions of a_f=2.5 mm (0.1 in) and b_f=15 mm (0.59 in). FRP mechanical properties were f_{fu}=2500 MPa (363 ksi) and E_f=165 GPa (23.9 Msi).

The angle α for BSMCFT was assumed to be equal to 28.5° for all the experimental programs [8]. To define the local bond stress-slip relationship (**Fig. 2b**) the following values were assumed: τ_0 = 20.1 MPa (2.9 ksi); $\delta_1 = 7.12$ mm (0.28 in) [8].

In NACI, to define average bond stress (τ_b) and effective strain (ε_{fe}) the following values were assumed: τ_b = 16.1 MPa (2.3 ksi) and ε_{fe} = 0.59% for the CFRP laminates [13], and τ_b = 6.9 MPa (1 ksi) and ε_{fe} = 0.4% for the CFRP rods [7].

When CFRP rods were used, the equivalent square cross-section was adopted in the calculations. The maximum dimension of aggregates (a_g) was assumed 25 mm (0.98 in) for all the experimental programs, since this information was not available in the majority of the original publications.

Fig. 5a shows the ratio between experimental results and analytical predictions from the BSMCFT formulation and NACI ($\lambda = V_{exp.} / \mathrm{V}_{ana.}$). The prediction of the results based on NACI are very high. The ratio between experiments and predictions is in average 1.47 with COV of 22%. For

SMCFT approach the average $V_{\exp.} / \mathrm{V}_{ana.}$ ratio is 1.09 with COV of 11%, which shows a better prediction than NACI approach.

A systematic trend in the error can be highlighted if the results are plotted in non-dimensional form, as it is shown in **Fig. 5b**, where the shear resistance is normalized by a force dimensional parameter $b_w d f_c^{'}$. In this figure, two lines limiting to $\pm 25\%$ the deviation of the predicted values from the experimental values are also represented, and it is easy to see that most of the results of NACI formulation are outside of these bounds, however it verified that almost all of the results of BSMCFT model are inside of these bounds.

The values of λ are also classified according to the modified version of the Demerit Points Classification (DPC) [21] proposed by Collins [22], where a penalty (PEN) is assigned to each range of λ parameter according to Table 2, and total of penalties (Total PEN) determines the performance of each analytical approach.

According to the results in Table 2 and **Fig. 5a**, the predictive performance of BSMCFT model is better than NACI, since BSMCFT model has a large number of predictions in the appropriate safety interval according to the DPC (Table 2), $\lambda \in [0.85 - 1.15[$: 60 samples with the BSMCFT and 13 samples with the NACI. According to results presented in Table 2, 80 and 36 samples are in the conservative interval ($\lambda \in [1.15 - 2[$), when using NACI and BSMCFT model, respectively. Both models have predictions on the unsafe interval (Table 2), ($\lambda \in [0.5 - 0.85[$): 4 samples with BSMCFT and 3 samples with NACI. The NACI also has predictions on the extremely conservative interval ($\lambda \geq 2$): 4 samples.

Based on the data presented in **Fig. 5** and Table 1 and 2 it can be concluded that the new approach predicts with high accuracy the shear strength of RC beams strengthened with CFRP laminates/rods applied according to the NSM technique.

Conclusion

To predict the shear resistance of the reinforced concrete (RC) beams shear strengthened according to the NSM technique, an analytical approach was, and its predictive performance was assessed by considering results available in literature.

The new approach is based on the simplified modified compression field theory (SMCFT), which takes into account the tensile stress factor in cracked concrete (β), and inclination of diagonal compressive strut (θ). For estimating the contribution of the CFRP laminates Bianco *et al.* formulations was selected. The experimental results of 100 beams with different configurations and percentage of CFRP laminates/rods were used to appraise the predictive performance of the developed approach. The new approach considers the inclination of the critical diagonal crack to determine the minimum number of FRP laminates/rods that cross the shear crack. By evaluating the ratio between the experimental results and the analytical predictions, an average value of 1.09 with a COV of 11% was obtained. Based on the results, it can be concluded that the new approach predicts with high accuracy the shear strength of RC beams shear strengthened with CFRP laminates/rods.

ACKNOWLEDGMENTS

The study presented in this paper is a part of the research project 38780, QREN, titled “CutInov – Innovative carbon fibre reinforced polymer laminates with capacity for a simultaneous flexural and shear/punching strengthening of reinforced concrete elements”, co-financed by the European

Regional Development Fund (FEDER) through the Operational Program COMPETE. The first author acknowledges the research grant provided by this project.

Notation

A_f	Area of the strip's cross section
A_2	Integration constant entering the expressions to evaluate the $V_{fi,eff}^{\max}$
A_3	Integration constant entering the expressions to evaluate the $V_{fi,eff}^{\max}$
C_3	Integration constant for the softening friction phase
J_1	Bond modeling constant
L_d	CDC length
L_p	Effective perimeter of the strip cross section
L_{Rfe}	Effective resisting bond length
L_{Rfi}	i^{th} strip resisting bond length
$\overline{L}_{Rfi}^{eq}$	Equivalent average resisting bond length
$\overline{L}_{Rfi}$	Average available resisting bond length
$N_{f,\mathrm{int}}^{l}$	Equivalent average resisting bond length
V_f^{tr}	Strip tensile rupture capacity
V_{fd}	Design value of the NSM shear strengthening contribution
$V_{fi,eff}^{\max}$	Maximum effective capacity
V_{f1}^{bd}	Maximum value of force transferable through bond by the given FRP NSM system
f_{ctm}^{*}	Value of concrete average tensile strength for values larger than which concrete fracture does not occur

f_{ctm}	Concrete average tensile strength
s_{xe}	Effective longitudinal crack spacing
α	Angle defining the concrete fracture surface
β	Factor accounting for the tensile stress in the cracked concrete
δ_1	Slip corresponding to the end of softening friction
δ_{Li}	Imposed slip at the loaded extremity of the i^{th} strip
δ_{Lu}	Imposed slip in correspondence of which the comprehensive peak force transmissible by $\bar{L}_{Rfi}^{eq}$ is attained
δ_{L1}	Value of δ_{Li} defining the end of the first phase of the bond-based constitutive law
ε_x	Longitudinal strain
$\varepsilon_{y\,yeild}$	Yield strain in transverse steel reinforcement
$\gamma_{\max}$	CDC opening angle for which the maximum effective capacity is attained
γ_{xy}	Shear strain
η	Reduction factor of the initial average available resisting bond length
λ	Constant entering the governing differential equation for elastic phase
τ_0	adhesive-cohesive initial bond strength
ψ	Constant necessary to evaluate the maximum effective capacity provided by the equivalent average resisting bond length

References

1. Bellamkonda, S.A., "*Modeling of Shear Strengthening of Reinforced Concrete Beams Retrofitted with Externally Bonded Fiber Reinforced Polymers*," Master thesis, Louisiana State University, 2013.
2. Blanksvärd, T., "*Strengthening of concrete structures by the use of mineralbased composites*," Luleå University of Technology, Sweden, 2009.

3. Vecchio, F.J., and Collins, M.P., "*The Modified Compression-Field Theory for Reinforced Concrete Elements Subjected to Shear."* ACI Journal Proceedings, 83 (2), 1986: pp. 219-231.

4. Bentz, E.C., Vecchio, F.J., and Collins, M.P., "*Simplified Modified Compression Field Theory for Calculating Shear Strength of Reinforced Concrete Elements.* " ACI Structural Journal, 103 (4), 2006.: pp. 614-624.

5. Dias, S.J.E., and Barros, J.A.O., "*Shear strengthening of RC T-section beams with low concrete using NSM CFRP laminates."* Journal Cement & Concrete Composites, 2011. 3(2): pp. 334-345.

6. De Lorenzis, L., and Nanni, A., "*Shear Strengthening of Reinforced Concrete Beams with Near-Surface Mounted Fiber-Reinforced Polymer Rods.*" ACI Structural Journal, 98 (1), 2001: pp. 60-68.

7. Nanni, A., Di Ludovico, M., and Parretti, R., "*Shear Strengthening of a PC Bridge Girder with NSM CFRP Rectangular Bars."* Advances in Structural Engineering, 7(4), 2004: pp. 97-109.

8. Bianco, V., Monti, G., and Barros, J.A.O., *Design formula to evaluate the NSM FRP strips shear strength contribution to a RC beam.* Composites Part B: Engineering, 56, 2014: pp. 960-971.

9. Sang-Yeol, P., "*Prediction of Shear Strength of R/C beams using Modified Compression Field Theory and ACI Code*." KCI Concrete Journal, 11(3), 1999: pp. 5-17.

10. Baghi, H., "*The effectivness of SHCC-FRP panles of the shear resistance of RC beams*," University of Minho, Portugal, 2015, PhD Thesis.

11. Bianco, V., Monti, G., and Barros, J.A.O., "*Theoretical model and computational procedure to evaluate the NSM FRP strips shear strength contribution to a RC beam."* ASCE Journal of Structural Engineering, 137(11), 2011: pp. 1359–1372.

12. ACI 440.2R-08 - Guide for the Design and Construction of Externally Bonded FRP Systems for Strengthening Concrete Structures: 2008.

13. Dias, S.J.E., and Barros, J.A.O., "*Performance of reinforced concrete T beams strengthened in shear with NSM CFRP laminates.*" Engineering Structures, 32(2), 2010: pp. 373-384.

14. Dias, S.J.E., and Barros, J.A.O., "*Shear strengthening of RC beams with NSM CFRP laminates: Experimental research and analytical formulation.*" Composite Structures, 99, 2013: pp. 477-490.

15. Dias, S.J.E., Barros, J.A.O., "*Shear Strengthening of T Cross Section Reinforced Concrete Beams by Near Surface Mounted Technique.*" ASCE Journal of Composites for Construction, 12(3), 2008: pp. 300-311.

16. Dias, S.J.E., "*Experimental and anlytical research in the shear strengthening of reinforced concreet beams using the near surface mounted technique with CFRP strips*," in *Department of Civil Engineering* 2008, University of Minho, Guimarães-Portugal, in Portugese.

17. Chaallal, O., Mofidi, A., Benmokrane, B., and Neale, K., "*Embedded Through-Section FRP Rod Method for Shear Strengthening of RC Beams: Performance and Comparison with Existing Techniques."* Composites for Construction, 15(3), 2011: pp. 374-383.

18. Rizzo, A., and De Lorenzis, L., "*Behaviour and capacity of RC beams strengthened in shear with NSM FRP reinforcement."* Construction and Building Materials, 3(4), 2009: pp. 1555-1567.

19. Islam, A.A., *Effective methods of using CFRP bars in shear strengthening of concrete girders.* Engineering Structures, 31(3), 2009: pp. 709-714.

20. Cisneros, D., Arteaga, A., De Diego, A., Alzate, A., Perera, R., *Experimental Study on NSM shear retrofiting of RC beams*, in 6th international conference on Composites in Civil Engineering, CICE 20122012: Rome, Italy.

21. Moraes Neto, B., Barros, J., Melo, G., *Model to Simulate the Contribution of Fiber Reinforcement for the Punching Resistance of RC Slabs*. Journal of Materials in Civil Engineering, 2014. 26(7).

22. Collins, M.P., *Evaluation of shear design procedures for concrete structures*, A Report prepared for the CSA technical committee on reinforced concrete design, 2001

List of Tables:

List of Figures:

Fig. 1*- Components of shear resistance for concrete beams without shear reinforcement: shear resistance in the compression zone (V_c); interface shear transfer by aggregate interlocking in the cracked concrete (V_a); and dowel action provided by the longitudinal reinforcement (V_d).*

Fig. 2*- Schematic representation of the Bianco et al. Model[11]; a) average-available-bond-length NSM strip and concrete prism of influence; b) adopted local bond stress-slip relationship; c) sections of the concrete prism; d) different failure mode of an NSM FRP laminate/rod subjected to an imposed end slip.*

Fig. 3*- a) available length reduction factor as function of the concrete average tensile strength, b) bond-based constitutive law for NSM FRP strips with different values of resisting bond length, c) assumed comprehensive constitutive law of the equivalent average available resisting bond length strip (Bianco et al.[8]) (1 kN= 0.22 kip and 1 mm= 0.04 in).*

Fig. 4*- Calculation procedure of BSMCFT.*

Fig. 5*- a) Ratio between experimental and predicted shear resistance; b) Predicted non-dimensional failure shear force of the beams, in compression with experimental values.*

Table 1- Summary of experimental and analytical results

Beam Label	$f_c^{'}$ (Mpa [ksi])	*Reinforcement*				$F_{\exp.}$ (kN [kips])	$\frac{F_{\exp.}}{F_{BSMCFT}}$	$\frac{F_{\exp.}}{F_{NACI}}$
		ρ_{sx}	θ_f	$\frac{\rho_y f_{y\,yield}}{f_c^{'}}$	$\frac{\rho_f f_{fu}}{f_c^{'}}$			
Dias and Barros [13, 14]								
C-R-I	39.7 (5.76)	0.028	-	0	0	207 (46.5)	1.11	1.78
2S-R-I		0.028	-	0.0143	0	304 (68.3)	1.18	1.71
7S-R-I		0.028	-	0.038	0	467 (105)	1.25	1.68
2S-4LV-I		0.028	90°	0.0143	0.056	337 (75.8)	1.09	1.45
2S-7LV-I		0.028	90°	0.0143	0.09	374 (84.1)	0.99	1.40
2S-10LV-I		0.028	90°	0.0143	0.12	397 (89.2)	1.03	1.28
2S-4LI45-I		0.028	45°	0.0143	0.055	393 (88.3)	1.18	1.81
2S-7LI45-I		0.028	45°	0.0143	0.9	422 (94.9)	1.05	1.50
2S-10LI45-I		0.028	45°	0.0143	0.13	446 (100.3)	1.09	1.32
2S-4LI60-I		0.028	60°	0.0143	0.49	386 (86.8)	1.22	1.70
2S-6LI60-I		0.028	60°	0.0143	0.076	394 (88.6)	1.13	1.43
2S-9LI60-I		0.028	60°	0.0143	0.11	413 (92.8)	1.01	1.27
4S-4LV-II		0.028	90°	0.0237	0.055	424 (95.3)	1.19	1.55
4S-7LV-II		0.028	90°	0.0237	0.09	427 (96.0)	1.12	1.39
4S-4LI45-II		0.028	45°	0.0237	0.055	442 (99.4)	1.17	1.71
4S-7LI45-II		0.028	45°	0.0237	0.09	478 (107.5)	1.07	1.48
4S-4LI60-II		0.028	60°	0.0237	0.048	444 (99.8)	1.22	1.66
4S-6LI60-II		0.028	60°	0.0237	0.076	458 (103.0)	1.16	1.44
Dias and Barros [5]								
C-R-III	18.6 (2.70)	0.028	-	0	0	147 (33.0)	1.08	1.88
2S-R-III		0.028	-	0.0304	0	226 (50.8)	1.08	1.62
4S-R-III		0.028	-	0.0508	0	304 (68.3)	1.17	1.68
2S-7LV-III		0.028	90°	0.0304	0.199	274 (61.6)	1.04	1.26
2S-4LI45-III		0.028	45°	0.0304	0.122	283 (63.6)	1.14	1.65
2S-7LI45-III		0.028	45°	0.0304	0.199	306 (68.8)	1.08	1.34
2S-4LI60-III		0.028	60°	0.0304	0.107	282 (63.4)	1.17	1.56
2S-6LI60-III		0.028	60°	0.0304	0.168	298 (67.0)	1.16	1.36
4S-7LV-III		0.028	90°	0.0508	0.199	315 (70.8)	1.05	1.21
4S-4LI45-III		0.028	45°	0.0508	0.122	347 (78.0)	1.17	1.64
4S-7LI45-III		0.028	45°	0.0508	0.199	356 (80.0)	1.07	1.32
4S-4LI60-III		0.028	60°	0.0508	0.107	346 (77.8)	1.19	1.57
4S-6LI60-III		0.028	60°	0.0508	0.168	362 (81.4)	1.19	1.39
Dias and Barros [15]								
C-R-IV	31.1 (4.51)	0.029	-	0	0	243 (54.6)	1.47	2.38
2S-R-IV		0.029	-	0.0182	0	315 (70.8)	1.35	1.94
6S-R-IV		0.029	-	0.0303	0	410 (92.2)	1.27	1.69

Beam Label	$f_c^{'}$ (Mpa [ksi])	*Reinforcement*				$F_{exp.}$ (kN [kips])	$\frac{F_{exp.}}{F_{BSMCFT}}$	$\frac{F_{exp.}}{F_{NACI}}$
		ρ_{sx}	θ_f	$\frac{\rho_y f_{y\,yield}}{f_c^{'}}$	$\frac{\rho_f f_{fu}}{f_c^{'}}$			
2S-3LV-IV		0.029	90°	0.0182	0.057	316 (71.0)	1.24	1.95
2S-5LV-IV		0.029	90°	0.0182	0.095	357 (80.2)	1.29	1.72
2S-8LV-IV		0.029	90°	0.0182	0.152	396 (89.0)	1.25	1.55
2S-3LI45-IV		0.029	45°	0.0182	0.057	328 (73.7)	1.11	1.68
2S-5LI45-IV		0.029	45°	0.0182	0.095	384 (86.3)	1.18	1.68
2S-8LI45-IV		0.029	45°	0.0182	0.152	382 (85.9)	1.05	1.47
2S-3LI60-IV		0.029	60°	0.0182	0.057	374 (74.1)	1.45	1.85
2S-5LI60-IV		0.029	60°	0.0182	0.085	392 (88.1)	1.28	1.85
2S-7LI60-IV		0.029	60°	0.0182	0.123	406 (91.3)	1.22	1.68
Dias [16]								
C-R-V	59.4 (8.61)	0.031	-	0	0	252 (44.5)	0.97	1.22
3S-R-V		0.031	-	0.0095	0	360 (80.9)	1.05	1.47
3S-6LV-V		0.031	90°	0.0095	0.025	387 (87.0)	0.91	1.29
3S-10LV-V		0.031	90°	0.0095	0.041	497 (111.7)	0.91	1.45
3S-5LI45-V		0.031	45°	0.0095	0.025	492 (110.6)	1.07	1.74
3S-9LI45-V		0.031	45°	0.0095	0.041	564 (126.8)	0.99	1.61
3S-5LI60-V		0.031	60°	0.0095	0.022	498 (112.0)	1.14	1.71
3S-8LI60-V		0.031	60°	0.0095	0.035	585 (131.5)	1.20	1.72
5S-R-VI		0.031	-	0.0143	0	410 (92.2)	1.05	1.46
5S-5LI45-VI		0.031	45°	0.0143	0.025	560 (125.9)	1.12	1.74
5S-9LI45-VI		0.031	45°	0.0143	0.041	627 (140.9)	1.03	1.62
5S-5LI60-VI		0.031	60°	0.0143	0.022	556 (125)	1.16	1.69
5S-8LI60-VI		0.031	60°	0.0143	0.035	655 (147.2)	1.24	1.74
Chaallal *et al.* [17]								
S0-CON-I	25.0 (3.62)	0.038	-	0	0	122 (40.7)	0.99	2.70
S1-CON-I		0.038	-	0.0812	0	351 (78.9)	1.07	0.99
S0-NSM-I		0.038	90°	0	0.54	331 (74.4)	1.13	1.70
S1-NSM-I		0.038	90°	0.0812	0.54	356 (80.0)	0.98	1.06
S3-CON-II	35.0 (5.07)	0.038	-	0.0386	0	295 (66.3)	0.98	1.68
S3-NSM-II		0.038	90°	0.0386	0.39	306 (68.8)	1.04	1.05
De Lorenzis and Nanni [6]								
BV	31.0 (4.50)	0.024	-	0	0	181 (40.7)	1.09	1.77
B90-7		0.024	90°	0	0.31	230 (51.7)	1.08	1.36
B90-5		0.024	90°	0	0.44	255 (57.3)	1.07	1.20
B45-7		0.024	45°	0	0.45	331 (74.4)	1.07	1.55
B45-5		0.024	45°	0	0.63	356 (80.0)	1.02	1.47
BSV		0.024	-	0.029	0	306 (68.8)	1.12	1.02
BS90-7A		0.024	90°	0.029	0.31	414 (93.1)	1.27	1.01

Beam Label	$f_c^{'}$ (Mpa [ksi])	*Reinforcement*				$F_{\exp.}$ (kN [kips])	$\frac{F_{\exp.}}{F_{BSMCFT}}$	$\frac{F_{\exp.}}{F_{NACI}}$
		ρ_{sx}	θ_f	$\frac{\rho_y f_{y\,yield}}{f_c^{'}}$	$\frac{\rho_f f_{fu}}{f_c^{'}}$			
Rizzo and De Lorenzis [18]								
C	29.3 (4.25)	0.044	-	0.0401	0	244 (54.8)	1.04	1.68
NR90-73-b		0.044	90°	0.0401	0.5191	297 (66.8)	1.04	1.42
NR90-45-b		0.044	90°	0.0401	0.8421	305 (68.6)	0.99	1.32
NR45-146-a		0.044	45°	0.0401	0.3671	326 (73.3)	1.11	1.70
NR45-73-a		0.044	45°	0.0401	0.7341	300 (67.4)	0.94	1.33
NL90-73-a		0.044	90°	0.0401	0.3097	345 (77.6)	1.20	1.22
NL45-146-a		0.044	45°	0.0401	0.219	310 (69.7)	1.06	1.21
Islam [19]								
Beam1	49.75 (7.20)	0.017	-	0.0338	0	365 (82.1)	0.86	0.91
Beam2		0.017	90°	0.0338	0.1404	454 (102)	0.93	0.93
Beam3		0.017	90°	0.0169	0.1404	427 (96.0)	1.09	1.66
Beam4		0.017	90°	0.0008	0.1404	436 (98.0)	1.28	1.37
Baghi [10]								
C-R	33 (4.77)	0.028	-	0	0	214 (48.1)	1.15	2.03
7S-R		0.028	-	0.046	0	530 (119.1)	1.15	1.78
NSM-3L45		0.028	45°	0	0.064	291 (65.4)	1.14	2.15
Cisneros *et al.* [20]								
Control	27.9 (4)		-	0.015	0	113 (25.4)	0.78	1.40
B90-6a	26.7 (3.8)		90°	0.016	0.41	170 (38.2)	1.05	1.16
B90-6b	24.1 (3.5)		90°	0.017	0.45	163 (36.6)	1.06	1.14
B90-3a	22.8 (3.3)		90°	0.018	0.24	117 (26.3)	0.84	1.14
B90-3b	26.0 (3.8)		90°	0.016	0.21	117 (26.3)	0.79	1.10
B45-6a	23.0 (3.3)		45°	0.018	0.67	180 (40.5)	1.08	1.17
B45-6b	28.5 (4.1)		45°	0.015	0.54	212 (47.7)	1.15	1.33
B45-3a	29.1 (4.2)		45°	0.015	0.26	189 (42.5)	1.06	1.43
B45-3b	23.9 (3.5)		45°	0.018	0.32	155 (34.8)	0.95	1.22
S90-6a	26.7 (3.9)		90°	0.015	0.30	189 (42.5)	1.17	0.95
S90-6b	24.1 (3.5)		90°	0.017	0.34	147 (33.0)	0.95	0.75
S90-3a	22.8 (3.3)		90°	0.018	0.18	117 (26.3)	0.84	0.97
S90-3b	26.0 (3.8)		90°	0.016	0.16	131 (29.5)	0.89	1.06
S45-6a	23.0 (3.3)		45°	0.018	0.50	183 (41.1)	1.09	0.66
S45-6b	28.5 (4.1)		45°	0.014	0.40	221 (49.7)	1.19	0.79
S45-3a	29.1 (4.2)		45°	0.014	0.20	206 (46.3)	1.16	1.15
S45-3b	23.9 (3.5)		45°	0.017	0.24	173 (38.9)	1.06	0.99
						Average	1.09	1.47
						COV	11%	22%

Table 2: Predictive performance of different approaches according to the modified version of the DPC

$\lambda = V_{\exp.} / \mathrm{V}_{ana.}$	*classification*	*Penalty*	*BSMCFT*		*NACI*	
			Nº samples	*Total*	*Nº samples*	*Total*
<0.5	Extremely Unsafe	10	0	0	0	0
[0.5-0.85[	Unsafe	5	4	20	3	15
[0.85-1.15[	Appropriate Safety	0	60	0	13	0
[1.15-2[	Conservative	1	36	36	80	80
$\geq$ *2.0*	Extremely Conservative	2	0	0	4	8
$\sum$ *PEN*			100	56	100	103

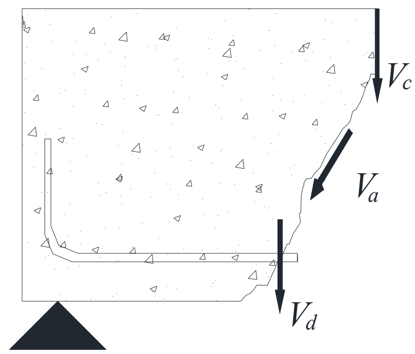

Fig. 1*- Components of shear resistance for concrete beams without shear reinforcement: shear resistance in the compression zone (V_c); interface shear transfer by aggregate interlocking in the cracked concrete (V_a); and dowel action provided by the longitudinal reinforcement (V_d).*

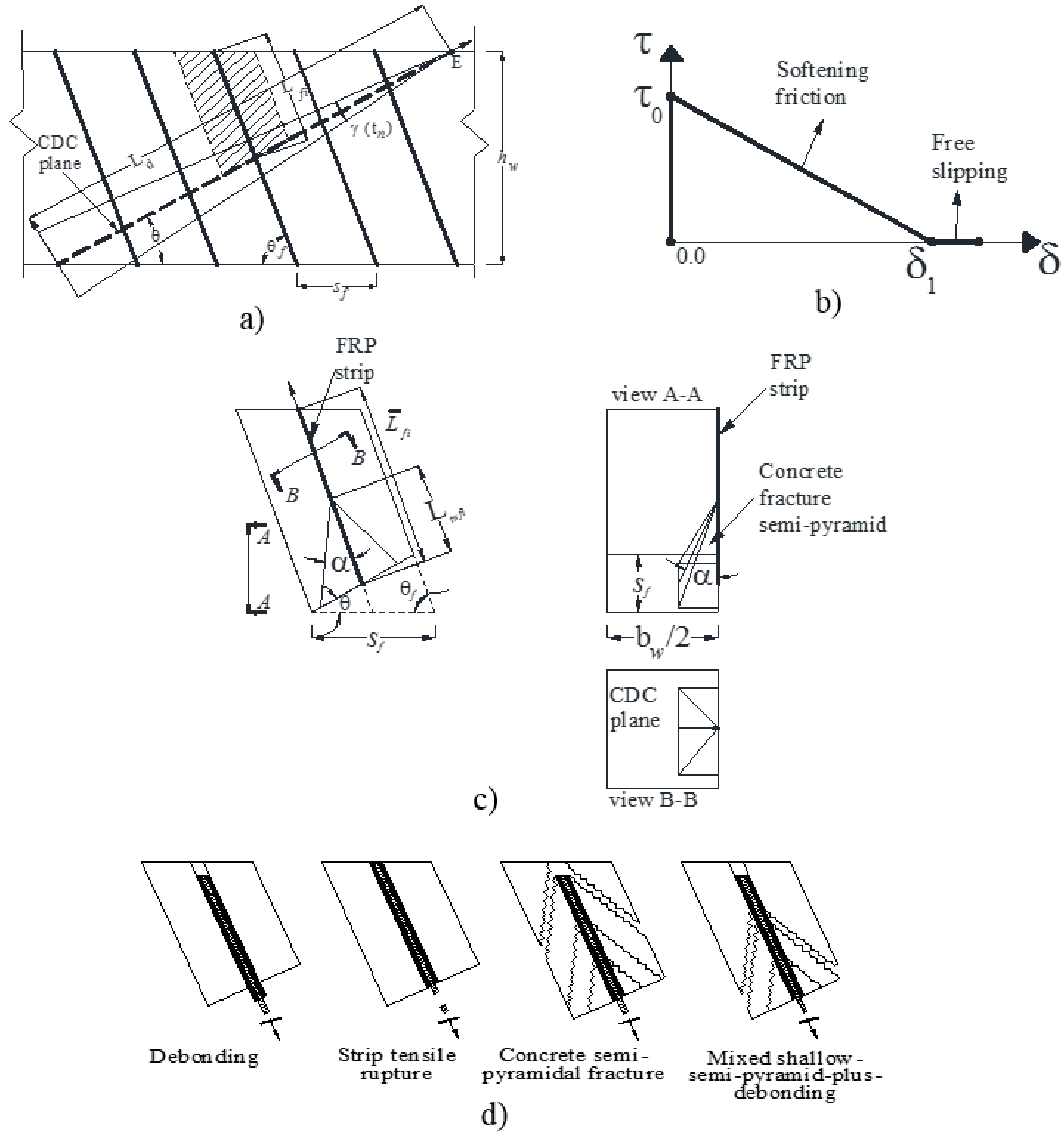

***Fig. 2**- Schematic representation of the Bianco et al. Model[11]; a) average-available-bond-length NSM strip and concrete prism of influence; b) adopted local bond stress-slip relationship; c) sections of the concrete prism; d) different failure mode of an NSM FRP laminate/rod subjected to an imposed end slip.*

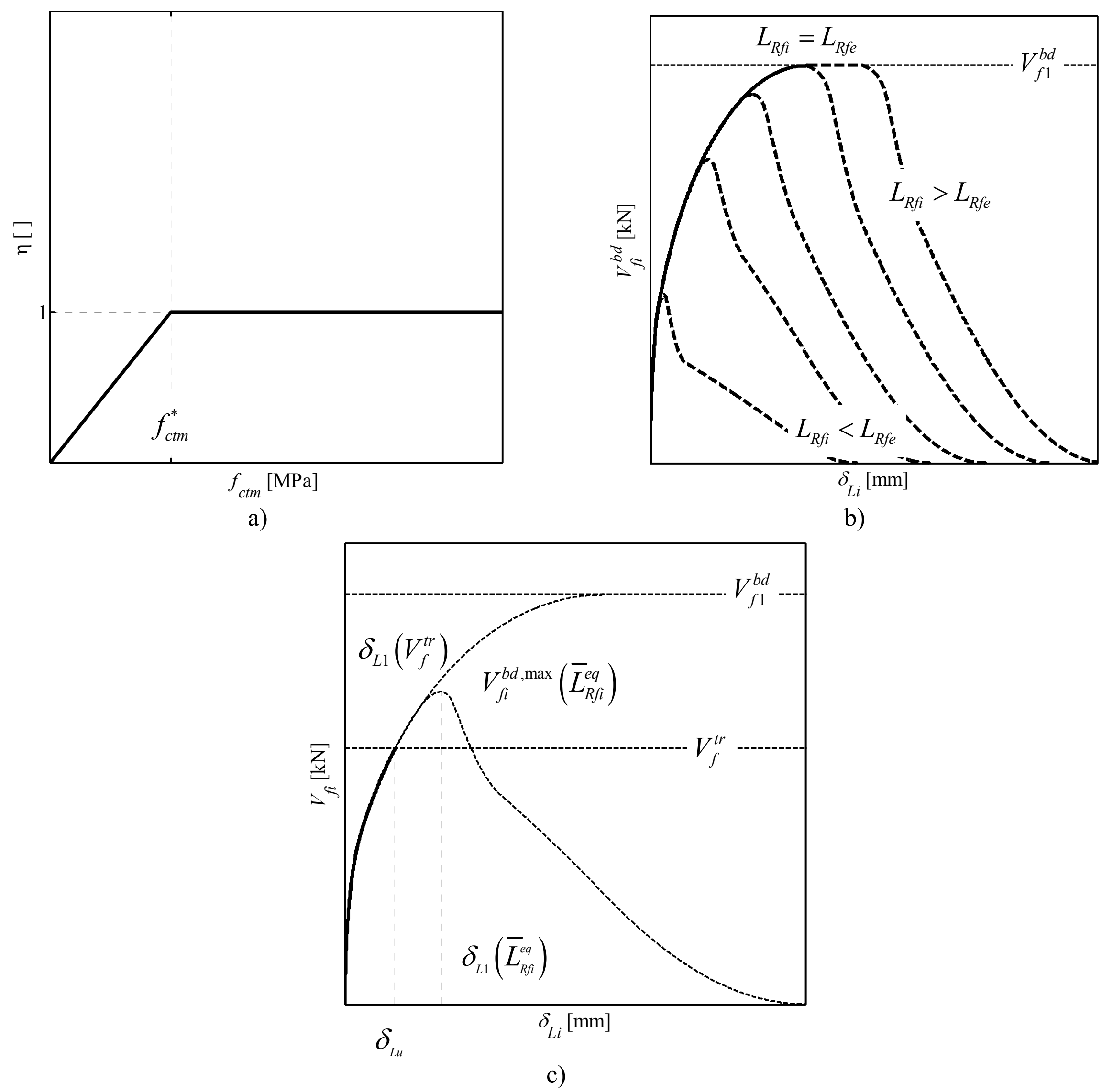

***Fig. 3**- a) available length reduction factor as function of the concrete average tensile strength, b) bond-based constitutive law for NSM FRP strips with different values of resisting bond length, c) assumed comprehensive constitutive law of the equivalent average available resisting bond length strip (Bianco et al.[8]) (1 kN= 0.22 kip and 1 mm= 0.04 in).*

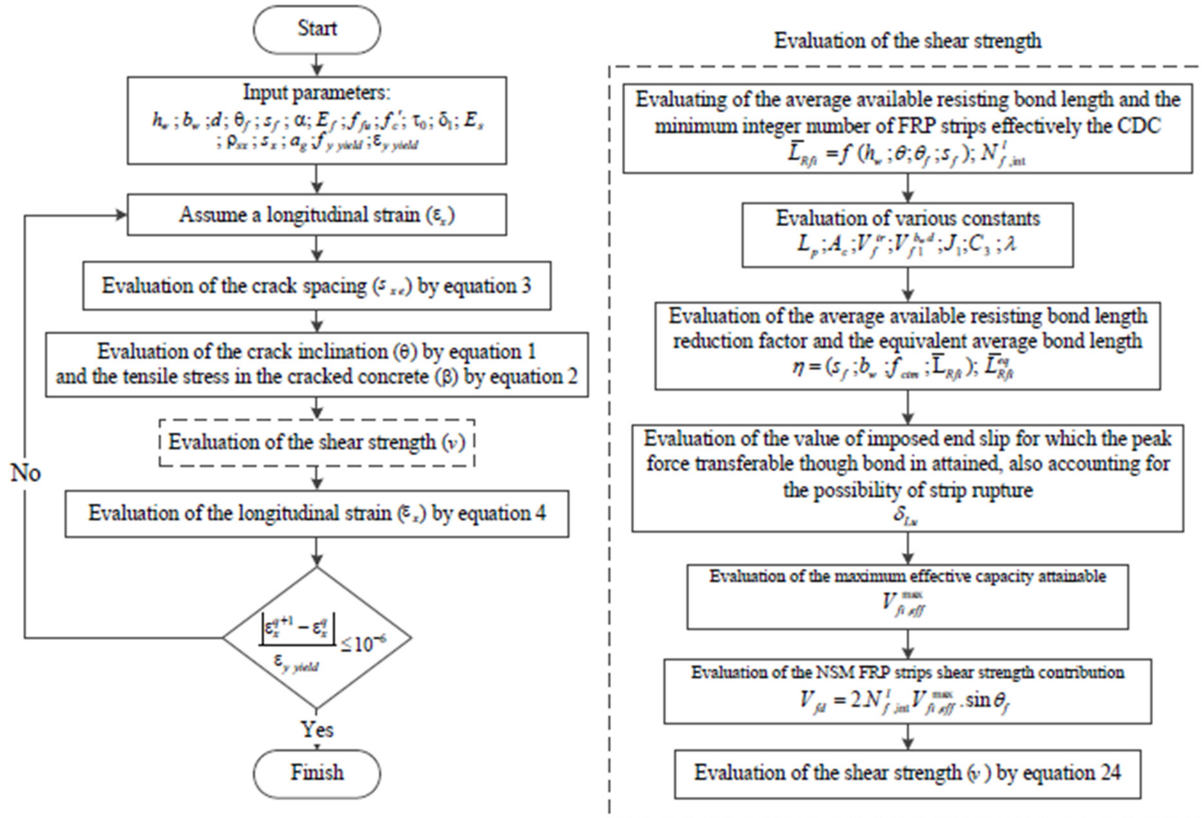

Fig. 4 *- Calculation procedure of BSMCFT*

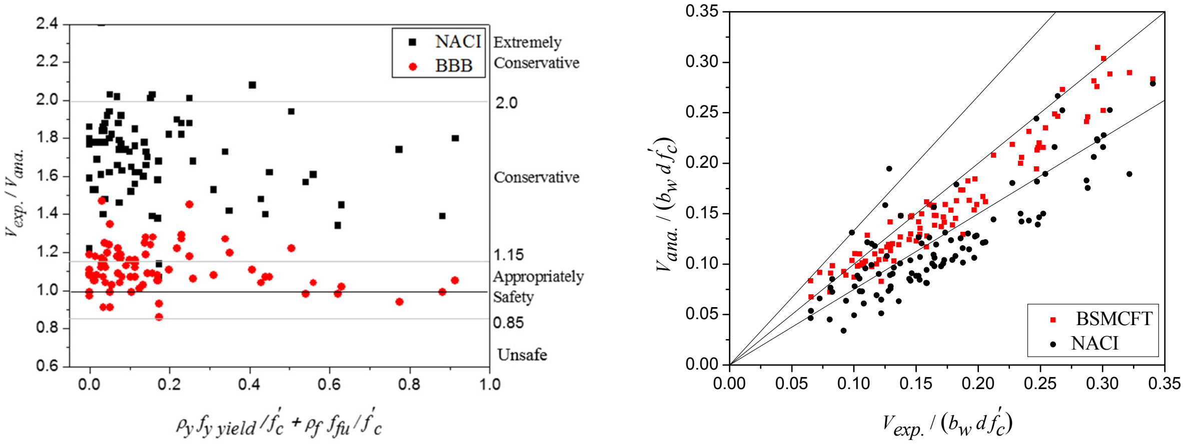

a) b)

***Fig. 5**- a) Ratio between experimental and predicted shear resistance; b) Predicted non-dimensional failure shear force of the beams, in compression with experimental values.*